

Bubbles and W-shaped solitons in Kerr media with fractional diffraction

Liangwei Zeng,^{1,2} Boris A. Malomed,^{3,4,*} Dumitru Mihalache,⁵
Yi Cai,^{1,2} Xiaowei Lu,^{1,2} Qifan Zhu,^{1,2} and Jingzhen Li^{1,2,†}

¹College of Physics and Optoelectronic Engineering, Shenzhen University, Shenzhen 518060, China

²Shenzhen Key Laboratory of Micro-Nano Photonic Information Technology,

Key Laboratory of Optoelectronic Devices and Systems of Ministry of Education and Guangdong Province,
College of Physics and Optoelectronic Engineering, Shenzhen University, Shenzhen 518060, China

³Department of Physical Electronics, School of Electrical Engineering,
Faculty of Engineering, and the Center for Light-Matter Interaction,
Tel Aviv University, P.O.B. 39040, Ramat Aviv, Tel Aviv, Israel

⁴Instituto de Alta Investigación, Universidad de Tarapacá, Casilla 7D, Arica, Chile

⁵Horia Hulubei National Institute of Physics and Nuclear Engineering, Magurele, Bucharest, RO-077125, Romania

(Dated: April 9, 2021)

We demonstrate that, with the help of a Gaussian potential barrier, dark modes in the form of a local depression (“bubbles”) can be supported by the repulsive Kerr nonlinearity in combination with fractional dimension. Similarly, W-shaped modes are supported by a double potential barrier. Families of the modes are constructed in a numerical form, and also by means of the Thomas-Fermi and variational approximations. All these modes are stable, which is predicted by computation of eigenvalues for small perturbations and confirmed by direct numerical simulations.

I. INTRODUCTION

Bright, dark, and gray solitons are fundamental modes that are known in various forms in nonlinear dispersive media [1–7], such as optical waveguides [8–16] and Bose-Einstein condensates [17–22]. Dark solitons, with zero-crossing shapes, are quiescent modes [10, 11, 23], while in the moving state they assume a complex (gray) shape, with a nonzero minimum of the absolute value [24–27]. Dark and gray solitons carry a topological charge, represented by the opposite signs of the finite-amplitude background fields on the two sides of these solitons. Nonlinear Schrödinger equations (NLSEs), with the attractive or repulsive sign of the cubic nonlinearity, are universal models producing soliton families of bright and dark types.

Varieties of fundamental and excited soliton states may be essentially expanded in spatially inhomogeneous settings [7, 28–32]. One of methods commonly used to create inhomogeneous nonlinear media is the introduction of linear lattice potentials [4, 33–38], which support families of gap solitons, such as fundamental [39], dipole [40] and vortex ones [41–45]. Another setup is based on the use of nonlinear lattices, i.e., spatially periodic modulations of the nonlinearity coefficient, which also help to build diverse soliton families [46], including fundamental, multipole, and vortical ones [47–49]. Furthermore, the self-repulsive cubic term, with the local strength growing fast enough from the center to periphery, makes it possible to maintain exceptionally robust species of self-trapped states [50–52], such as solitary vortices [53–56], soliton gyroscopes [57], *hopfions* (twisted vortex rings) [58], vortex clusters [59, 60], and flat-top solitons [61, 62].

Depending on the form of the self-repulsive nonlinearity, dark modes also may exist in the form of “bubbles”, i.e., quiescent real states with a nonzero local minimum of the amplitude [63–65]. Unlike dark solitons, bubbles do not carry a topological charge.

A particular species of spatial modes produced by NLSEs is represented by W-shaped solitons, so named because of their shape with two local minima [66–72]. Physical settings that support W-shaped solitons include nonlinear fibers with higher-order effects [66, 67], optical materials with self-induced transparency [68], negative-refractive-index materials [71], as well as the media with inhomogeneous repulsive nonlinearity [72].

An essential extension of the class of Schrödinger equations was introduced by Laskin [73–76], in the form of the fractional Schrödinger equation, which includes the fractional derivative, instead of the usual second-order differential term. The model was developed as one for a quantum particle moving by way of *Lévy flights* (random jumps). The addition of the cubic term to the equation leads to the concept of the nonlinear fractional Schrödinger equation (NLFSE). In the context of the quantum many-body theory, NLFSE may be considered as an appropriate equation of the Gross-Pitaevskii (mean-field) type for a Bose-Einstein condensate of such particles [77, 78]. Further, NLFSE has drawn much interest due to possibilities of its experimental realization in the classical form, in condensed matter physics [79, 80] and optics [81]. Solitons produced by NLFSEs have been predicted in various forms [82–99], including “accessible” solitons [82, 83] and ones supported by nonlinear lattices [84, 99], symmetry-breaking states [86–89], gap solitons [90], solitary vortices [91, 92], multi-peak modes [93], soliton clusters [94, 95], coupled solitons [96, 97], discrete ones [98], and localized pulses in fractional complex Ginzburg-Landau equation [100].

Although many soliton species have been found as so-

* malomed@tauex.tau.ac.il

† lijz@szu.edu.cn

lutions of NLFSEs, bubble-type and W-shaped modes were not yet addressed in the case of equations of the fractional order. Such states, supported by the repulsive cubic nonlinearity, are the subject of the present work. We demonstrate that they can be stabilized by a Gaussian potential barrier (or two barriers, for the W-shaped states) added to the setting.

The rest of the paper is organized as follows. In Sec. II, we present the model and formulate the linear stability analysis for it. The same section includes two analytical methods, *viz.*, a crude Thomas-Fermi (TF) approximation and a more accurate variational approach. Numerical results for the bubbles and W-shaped modes are reported in two parts of Sec. III. The paper is concluded by Sec. IV.

II. THE MODEL AND ANALYTICAL APPROXIMATIONS

A. Basic equations

The NLFSE is introduced in terms of the spatial-domain light propagation, with field amplitude E , along axis z in a waveguide with the defocusing Kerr nonlinearity, under the action of fractional diffraction in the transverse direction, x . In the scaled form, the equation takes the form of

$$i \frac{\partial E}{\partial z} = \frac{1}{2} \left(-\frac{\partial^2}{\partial x^2} \right)^{\alpha/2} E + V(x)E + 4|E|^2 E, \quad (1)$$

where $(-\partial^2/\partial x^2)^{\alpha/2}$ is the fractional Laplacian, determined by the Lévy index α . In fact, the fractional derivative is defined as an integral operator,

$$\left(-\frac{\partial^2}{\partial x^2} \right)^{\alpha/2} E = \frac{1}{2\pi} \int_{-\infty}^{+\infty} dp |p|^\alpha \int_{-\infty}^{+\infty} d\xi e^{ip(x-\xi)} E(\xi). \quad (2)$$

The strength of the self-repulsive nonlinearity in Eq. (1) is fixed to be 4 by means of an obvious rescaling of E .

The implementation of the fractional diffraction, modeled by Eq. (2), in optics was elaborated by Longhi [81]. It can be realized in a Fabry-Perot resonator, into which two lenses and two phase masks are inserted, with the phase shift $f(x)$, introduced by the mask, which depends on the transverse coordinate, x , as $f(x) \sim |x|^\alpha$. In that case, the variable z in Eq. (1) is proportional to the number of circulations of light beams in the resonator. It is also relevant to mention early works [101] and [102], which proposed the implementation of the fractal diffraction by means of optical filters.

In works on the NLFSE with the attractive cubic term, which corresponds to the negative coefficient in front of the cubic term in Eq. (1), the Lévy index takes the values $1 < \alpha \leq 2$, because at $\alpha \leq 1$ such an equation gives rise to collapse, hence all stationary solutions are unstable. On the other hand, solitons may be stabilized by a self-repulsive quintic term added to the NLFSE [91], as well

as by a trapping potential [93], which makes it possible to obtain stable solutions at $\alpha \leq 1$ (e.g., for $\alpha = 1$ [91] and $0.7 < \alpha \leq 1$ [93]).

The potential in Eq. (1), which supports bubble modes, is adopted in the form of a Gaussian barrier, with height A and width W :

$$V(x) = A \exp\left(-\frac{x^2}{2W^2}\right). \quad (3)$$

In optics, it can be readily realized by means of an inhomogeneity of the refractive index. Note that, while potential barriers repel bright solitons, they attract dark modes. Accordingly, to produce W-shaped states, the potential will be taken as a pair of Gaussian barriers,

$$V(x) = A \left\{ \exp\left[-\frac{(x-x_0)^2}{2W^2}\right] + \exp\left[-\frac{(x+x_0)^2}{2W^2}\right] \right\}, \quad (4)$$

where the constant $x_0 > 0$ controls the separation between them.

Stationary states with real propagation constant k are looked for as solution to Eq. (1) in the form of

$$E(x, z) = U(x) \exp(ikz). \quad (5)$$

The substitution of this expression in Eq. (1) leads to an equation for real function $U(x)$:

$$-kU = \frac{1}{2} \left(-\frac{\partial^2}{\partial x^2} \right)^{\alpha/2} U + V(x)U + 4U^3. \quad (6)$$

In particular, dark modes are supported by the modulationally stable flat background, represented by constant solutions of Eq. (6) with $V(x) = 0$,

$$U_b = \sqrt{-k}/2, \quad (7)$$

which exist for all negative values of k .

Note that Eq. (6), combined with the definition of fractional-diffraction operator (2), is invariant with respect to rescaling,

$$\begin{aligned} \tilde{x} &\equiv X_0^{-1}x, \quad \tilde{k} \equiv X_0^\alpha k, \\ \tilde{V}(\tilde{x}) &\equiv X_0^\alpha V(X_0\tilde{x}), \quad \tilde{U}(\tilde{x}) \equiv X_0^{\alpha/2} U(X_0\tilde{x}), \end{aligned} \quad (8)$$

with arbitrary scaling factor X_0 . The invariance makes it possible to fix either amplitude or width of the potential barrier (3) (similarly, one can fix one parameter for the double barrier (4)). Nevertheless, presenting numerical results below, we independently vary the constants k , A , and W , as the variation of any of them is a natural scenario for experiments.

Equation (1) conserves the total norm, which represents the integral power of the light beam in the underlying optical model:

$$P = \int_{-\infty}^{+\infty} |E(x)|^2 dx. \quad (9)$$

For stationary dark modes, P diverges because of the contribution of the nonvanishing background, while an appropriate characteristic of the modes is the *power defect*,

$$\Delta P \equiv \int_{-\infty}^{+\infty} [U_b^2 - U^2(x)] dx, \quad (10)$$

where U_b^2 is the background density supporting the dark states, given by Eq. (7).

B. The Thomas-Fermi (TF) approximation

The simplest analytical approximation for stationary modes, which, actually, completely ignores the fractional dimension, dropping the (fractional) derivative term in Eq. (6), is the TF approximation, which is widely applied to the consideration of Bose-Einstein condensates with the self-repulsive nonlinearity [103]. In this approximation, Eq. (6) yields

$$U_{\text{TF}}^2(x) = (1/4) [|k| - V(x)], \quad (11)$$

provided that the maximum value of the potential is subject to condition $V_{\text{max}} < |k|$ (recall that we consider $k < 0$). In the case of $V_{\text{max}} > |k|$, the TF approximation takes the form including an empty (zero-field) segment:

$$U_{\text{TF}}^2(x) = \begin{cases} (1/4) [|k| - V(x)], & \text{at } V(x) < |k|, \\ 0, & \text{at } V(x) > |k|. \end{cases} \quad (12)$$

In the case of potential barrier (3), the empty “hole” is the central segment, $|x| < W\sqrt{2 \ln(A/|k|)}$. However, numerically found profiles of the bubbles, displayed below (see Figs. 2(a,d,g)), do not feature any “hole”, even in an approximate form. Thus, the fractional diffraction operator supports profiles that are quite different from their TF counterparts.

The TF approximation produces the corresponding values of the power defect, ΔP . In particular, in the case of $A < |k|$, the substitution of expression (11), with $V(x)$ taken as per Eq. (3), yields a simple expression, which does not depend on k :

$$(\Delta P_{\text{TF}})_{A < |k|} = \sqrt{\pi/8} AW. \quad (13)$$

In the case of the double potential barrier (4), the TF approximation yields a result that is twice as large, *viz.*,

$$(\Delta P_{\text{TF}})_{\text{double}} = \sqrt{\pi/2} AW. \quad (14)$$

It is shown below in Figs. 2(c,f) that, although the TF prediction of the bubbles’ shapes is not accurate, the expression (13) correctly predicts essential features of the dependence of ΔP on parameters.

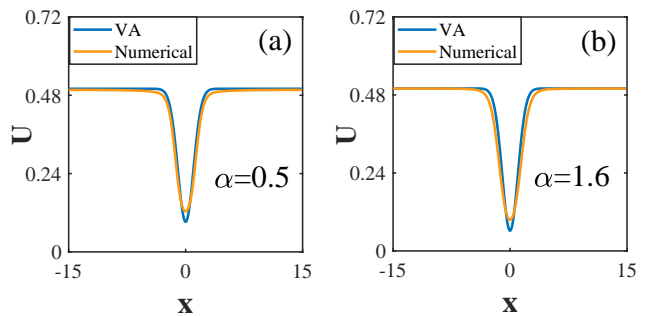


FIG. 1. Numerically obtained profiles of bubbles and their variational counterparts (yellow and blue lines, respectively), supported by the potential barrier (3), for values of the Lévy index $\alpha = 0.5$ (a) and 1.6 (b). Parameters of the potential barrier are $A = 2$, $W = 1$, and $k = -1$.

C. The variational approximation

For a fixed value of k and, accordingly, the background value of U fixed as per Eq. (7), the bubble solution may be looked for as

$$U(x) = \left(\sqrt{-k}/2 \right) - u(x), \quad (15)$$

with a positive localized field $u(x)$ satisfying the complementary equation,

$$\begin{aligned} \frac{1}{2} \left(-\frac{\partial^2}{\partial x^2} \right)^{\alpha/2} u + (V(x) - 2k)u - 6\sqrt{-k}u^2 + 4u^3 \\ = \frac{\sqrt{-k}}{2} V(x). \end{aligned} \quad (16)$$

The fact that the Eq. (16) can be derived from the Lagrangian,

$$\begin{aligned} L = \frac{1}{8\pi} \int_{-\infty}^{+\infty} dp |p|^\alpha \int_{-\infty}^{+\infty} dx \int_{-\infty}^{+\infty} d\xi e^{ip(x-\xi)} u(\xi) u(x) \\ + \int_{-\infty}^{+\infty} dx \left[\left(\frac{V}{2} - k \right) u^2 - 2\sqrt{-k}u^3 + u^4 - \frac{\sqrt{-k}V}{2} u \right], \end{aligned} \quad (17)$$

where the definition (2) for the fractional derivative is used, suggests one to apply the variational approximation, similar to how it was used for bright solitons of the NLFSE with the cubic self-attraction in Ref. [100]. A natural variational ansatz for the bubble is a Gaussian with amplitude $a > 0$ considered as a free parameter:

$$u_{\text{ans}}(x) = a \exp \left(-\frac{x^2}{2W^2} \right). \quad (18)$$

A more general ansatz can be used too, with its width treated as another free parameter, rather than fixed to be equal to W , but the respective generalization leads to quite cumbersome variational equations.

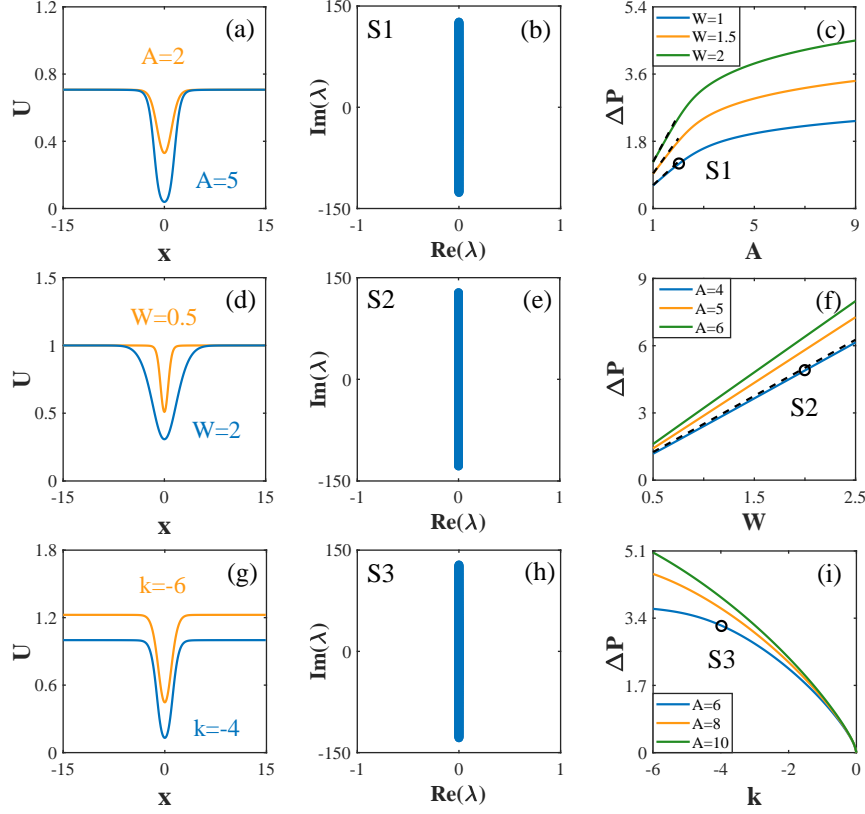


FIG. 2. (a) Profiles of typical bubble solutions supported by the potential barrier (3) with different values of A and fixed parameters $W = 1$, $k = -2$. (b) Eigenvalues of small perturbations around the bubble with $A = 2$, $W = 1$, $k = -2$. (c) Power defect ΔP of the bubble solutions vs. amplitude A of the potential barrier, see Eqs. (10) and (13), for different values of width W at a fixed value of the propagation constant, $k = -2$. The black dashed lines in panels (c,f) are the TF predictions, as given by Eq. (13). (d) Bubble profiles with different values of W at $A = 4$, $k = -4$. (e) Eigenvalues of small perturbations at $A = 4$, $W = 2$, $k = -4$. (f) ΔP vs. W for different values of A at $k = -4$. (g) Bubble profiles with different values of k at $A = 6$, $W = 1$. (h) Eigenvalues of small perturbations at $A = 6$, $W = 1$, $k = -4$. (i) ΔP vs. k for different values of A at $W = 1$. The evolution of perturbed propagations of the bubbles marked by S1–S3 is displayed in Figs. 4(a–c), respectively. Except for the left panel of Fig. 1, the Lévy index α in Eq. (1) is fixed as $\alpha = 1.6$.

The substitution of ansatz (18) in Lagrangian (17) and subsequent integration yields the effective Lagrangian:

$$\frac{1}{\sqrt{\pi}W}L_{\text{eff}} = -\frac{\sqrt{-k}}{2}Aa - \sqrt{-\frac{8k}{3}}a^3 + \frac{1}{\sqrt{2}}a^4 + \left[\frac{\Gamma((\alpha+1)/2)}{4\sqrt{\pi}}W^{-\alpha} - k + \frac{A}{\sqrt{6}} \right] a^2, \quad (19)$$

where Γ is the Euler's Gamma-function. The value of the amplitude a in ansatz (18) is predicted by the Euler-Lagrange equation, $dL_{\text{eff}}/da = 0$, which takes the form of

$$\sqrt{2}a^3 - \sqrt{-6k}a^2 + \left[\frac{\Gamma((\alpha+1)/2)}{4\sqrt{\pi}}W^{-\alpha} - k + \frac{A}{\sqrt{6}} \right] a - \frac{\sqrt{-k}}{4}A = 0. \quad (20)$$

With a found as a solution of this cubic equation, one can produce the variational prediction for the power defect,

substituting expressions (15) and (18) in Eq. (10):

$$\Delta P_{\text{var}} = 2\sqrt{-\pi k}Wa - \sqrt{\pi}Wa^2. \quad (21)$$

D. The formulation of the stability analysis

Stability of the stationary modes was investigated, as usually, by taking perturbed ones as

$$E = [U(x) + p(x)\exp(\lambda z) + q^*(x)\exp(\lambda^* z)]\exp(ikz), \quad (22)$$

where $p(x)$ and $q^*(x)$ are eigenmodes of small perturbations with instability growth rate λ , the asterisk standing for complex conjugate [4]. Substituting this ansatz in Eq. (1) and linearization leads to the eigenvalue problem

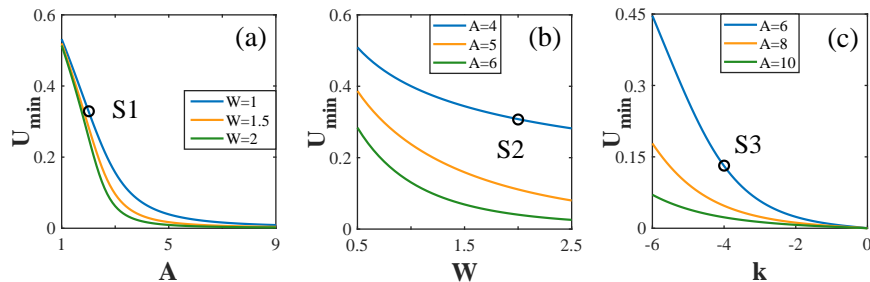


FIG. 3. (a) The minimal value U_{\min} of the bubble solution, supported by the potential barrier (3), vs. A for different values of W at $k = -2$. (b) U_{\min} vs. W for different values of A at $k = -4$. (c) U_{\min} vs. k for different values of A at $W = 1$.

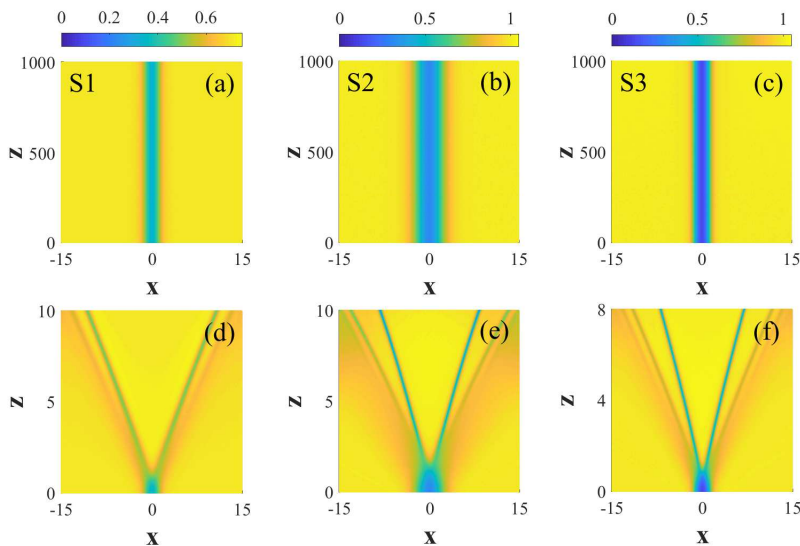


FIG. 4. Stable propagation of perturbed bubbles supported by the potential barrier (3): (a) at $A = 2$, $W = 1$, $k = -2$; (b) at $A = 4$, $W = 2$, $k = -4$; (c) at $A = 6$, $W = 1$, $k = -4$. Panels (d,e,f) display diffraction of the same inputs as in (a,b,c), respectively, but without the potential barrier ($A = 0$).

based on equations

$$\begin{cases} i\lambda p = +\frac{1}{2} \left(-\frac{\partial^2}{\partial x^2} \right)^{\alpha/2} p + (k + V)p + 4U^2(2p + q), \\ i\lambda q = -\frac{1}{2} \left(-\frac{\partial^2}{\partial x^2} \right)^{\alpha/2} q - (k + V)q - 4U^2(2q + p). \end{cases} \quad (23)$$

(in the theory of Bose-Einstein condensates, they are called Bogoliubov-de Gennes equations [103]). The stationary solution is stable if all the eigenvalues λ produced by Eq. (23) are pure imaginary ones.

III. NUMERICAL RESULTS

Numerical solutions of Eq. (6) were constructed by means of the modified squared-operator method [4]. Stability and instability domains for families of stationary

states were identified by means of eigenvalues produced by a numerical solution of Eq. (23) and verified by direct numerical simulations of Eq. (1) for the perturbed evolution of the same states, performed with the help of the split-step fast-Fourier-transform method. The numerical findings are presented below, chiefly, for $\alpha = 1.6$, as a characteristic value of the Lévy index that is essentially different from $\alpha = 2$, which corresponds to the usual NLSE. To illustrate the generality of the obtained results, some of them are additionally displayed, in Fig. 1, for a very different value of the Lévy index, $\alpha = 0.5$.

A. Bubbles

Typical profiles of bubbles for the above-mentioned values of the Lévy index, $\alpha = 0.5$ and 1.6 , are displayed in Fig. 1, along with their counterparts predicted by the variational approximation, as per Eqs. (15), (18), and

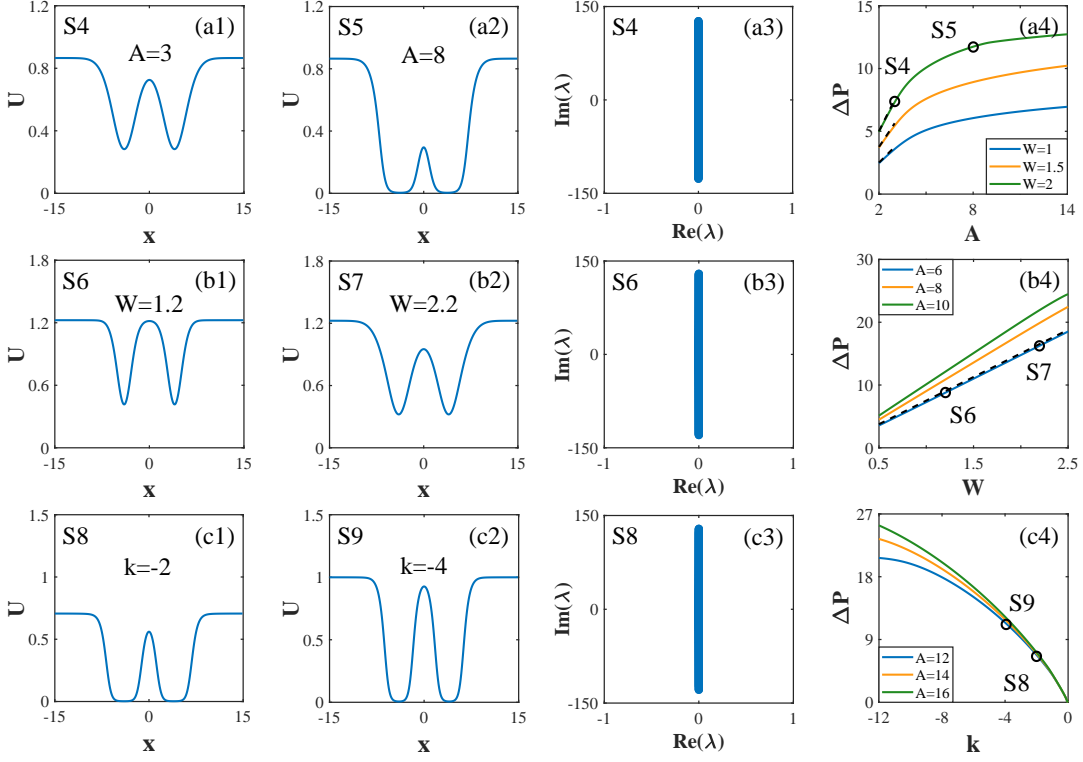


FIG. 5. The same as in Fig. 2, but for W-shaped dark modes supported by the double potential barrier (4). Profiles of the modes at $W = 2$, $k = -3$: (a1) with $A = 3$; (a2) with $A = 8$. (a3) The spectrum of perturbation eigenvalues for the W-shaped mode at $A = 3$, $W = 2$, $k = -3$. (a4) $\Delta P(A)$ with different values of W at $k = -3$. The black dashed lines in panels (a4,b4) are the TF predictions (14). Profiles of the mode at $A = 6$, $k = -6$: (b1) for $W = 1.2$; (b2) for $W = 2.2$. (b3) The spectrum of eigenvalues for $A = 6$, $W = 1.2$, $k = -6$. (b4) $\Delta P(W)$ for different values of A at $k = -6$. Profiles of the modes at $A = 12$, $W = 1.4$: (c1) for $k = -2$; (c2) for $k = -4$. (c3) The spectrum of perturbation eigenvalues for $A = 12$, $W = 1.4$, $k = -2$. (c4) $\Delta P(k)$ for different values of A at $W = 1.4$. The propagations of perturbed modes marked by S4, S6, and S8 are displayed in Figs. 7(a-c), respectively. In this and the other figures, $x_0 = 4$ is fixed in Eq. (4).

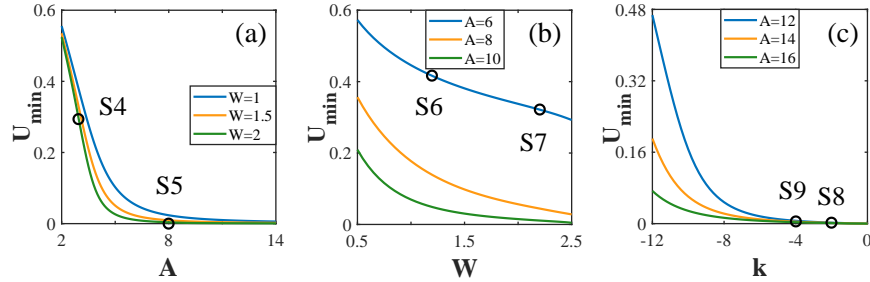


FIG. 6. The same as in Fig. 3, but for the W-shaped modes. (a) U_{\min} of the modes versus A for different values of W at $k = -3$. (b) U_{\min} versus W for different values of A at $k = -6$. (c) U_{\min} versus k for different values of A at $W = 1.4$.

(20). It is seen that the approximation predicts the profiles with good accuracy.

Typical profiles of bubbles, spectra of eigenvalues of small perturbations around them, and characteristics of the bubble-solution families, in the form of the dependence of the respective power defect (10) on the parameters, are displayed in Fig. 2. In particular, the profile and

eigenvalue spectrum shown in panels (a) and (b) represent the bubble marked by S1 in (c). Note that ΔP increases with A in panel (c), at different values of width W of the Gaussian potential barrier (3). This dependence agrees with panel (a), where the minimum level $U(x = 0) \equiv U_{\min}$ of the bubble's field decreases, quite naturally, with the increase of A .

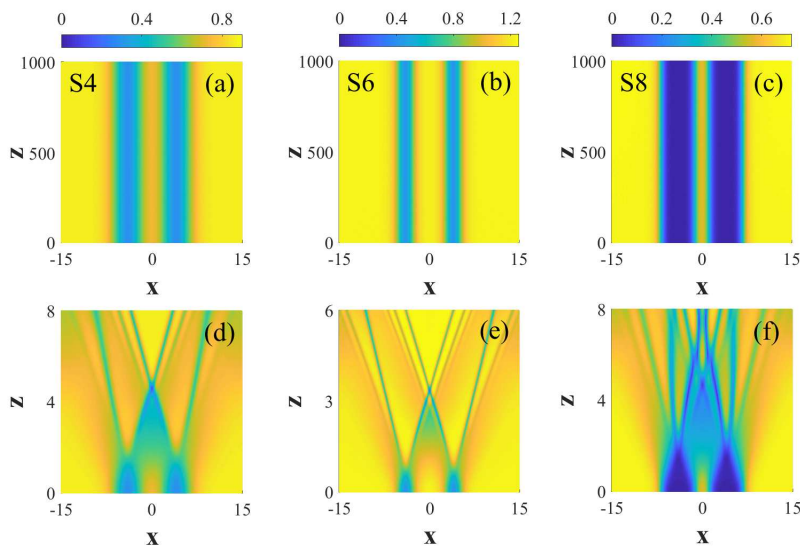


FIG. 7. The stable propagation of perturbed W-shaped dark modes: (a) at $A = 3$, $W = 2$, $k = -3$; (b) at $A = 8$, $W = 1.2$, $k = -6$; (c) at $A = 12$, $W = 1.4$, $k = -2$. (d,e,f) Diffraction of the same inputs in the case when the double Gaussian potential barrier is removed.

Further, the dependence $\Delta P(W)$ for different values of A is displayed in Fig. 2(f), which shows that ΔP increases with W almost linearly for different values of A . This property agrees with panel (d), which shows that, also naturally, U_{\min} decreases with the increase of width W of the repulsive barrier, and the bubble's width increases, following the increase of W . The profile and eigenvalue spectrum shown in panels (d) and (e) of Fig. 2 represent the bubble marked by S2 in Fig. 2(f). Note that the nearly linear dependence $\Delta P(A)$ in the region of $A < |k|$ in Fig. 2(c), and the linear dependence $\Delta P(W)$ in Fig. 2(f) are consistent with the simple TF prediction, given by Eq. (13).

The dependence $\Delta P(k)$ is presented in Fig. 2(i), which demonstrates that ΔP increases with the increase of $|k|$ for different values of A . The respective typical profiles of the bubbles with different k are plotted in Fig. 2(g), showing that U_{\min} increases with $|k|$, while the bubble's width remains nearly constant. The profile and eigenvalue spectrum shown in panels (g) and (h) of Fig. 2 represent the bubble marked by S3 in Fig. 2(i).

The minimum value U_{\min} being an essential characteristic of the bubble, we display its dependence on A for different values of W in Fig. 3(a), from which one can clearly see that (as mentioned above) U_{\min} decreases with the increase of A . The same property is predicted by the TF approximation, as long as A remains smaller than $|k|$, as it follows from Eqs. (11) and (3):

$$(U_{\min})_{\text{TF}} = (1/2)\sqrt{|k| - A}. \quad (24)$$

Beyond the framework of the TF approximation, U_{\min} depends on the width of the potential barrier, W , naturally decreasing with the increase of W , as seen in Fig. 3(b).

Next, the dependence $U_{\min}(W)$ is plotted in Fig. 3(b), where U_{\min} decreases with the increase of W , and Fig. 3(c) demonstrates that U_{\min} increases (i.e., the bubble becomes more shallow) with the increase of $|k|$. In all cases, the values of U_{\min} are lower for larger A , which is explained by the fact that the potential barrier (3) with larger A provides a stronger repulsive effect.

The eigenvalue spectra, examples of which are displayed in Figs. 2(b,e,h), demonstrate that all the bubble solutions are stable. Further, perturbed long-distance propagation (up to $z = 1000$, which is tantamount to ~ 200 Rayleigh (diffraction) lengths of the respective stationary solutions) of the bubbles marked by S1–S3 in Figs. 2(c,f,i) is displayed in Figs. 4(a–c), respectively, which confirms the predicted stability. The Rayleigh length can be identified in Figs. 4(d–f), which displays the diffraction of the same inputs in the case when the potential barrier (3) is removed in Eq. (1).

B. W-shaped solitons

Typical profiles of W-shaped dark modes, supported by the double potential barrier (4), and the dependence of the respective power defect ΔP on parameters are displayed in Fig. 5. It is observed that the dependences are qualitatively similar to their counterparts for the bubbles, shown above in Fig. 2. The profiles of the W-shaped modes marked by S4 and S5 in Fig. 5(a4) are presented in Figs. 5(a1) and (a2), respectively, and the spectrum of the perturbation eigenvalues for the former solution is shown in panel (a3). Similarly, the profiles of the modes marked by S6 and S7 in Fig. 5(b4) are presented in Figs. 5(b1) and (b2), respectively, and the

eigenvalue spectrum for the former one is shown in Fig. 5(b3). Next, the profiles of the W-shaped modes marked by S8 and S9 in Fig. 5(c4) are presented in Figs. 5(c1) and (c2), respectively, and the eigenvalue spectrum of the former one is presented in Fig. 5(c3).

In Figs. 6(a), (b), and (c) we plot, severally, the minimum value U_{\min} of the W-shaped mode as a function of A for different values of W , as a function of W for different values of A , and as a function of k for different values of A . These dependence are qualitatively similar to their counterparts for the bubbles displayed in Fig. 3, and can be qualitatively explained by means of the same arguments that are mentioned above for the bubbles.

Similar to the bubbles, the W-shaped modes are also completely stable. This conclusion is illustrated by examples of spectra of perturbation eigenvalues presented in Figs. 5(a3,b3,c3). The predicted stability is confirmed by numerical simulations of the propagations of perturbed modes marked by S4, S6, and S8 in Figs. 7(a-c), respectively. For the sake of comparison, the diffraction of the same inputs in the absence of the double potential layer is displayed in Figs. 7(d,e,f).

IV. CONCLUSION

We have constructed the bubble and W-shaped modes, supported, respectively, by the single and double Gaus-

sian potential barrier, in the medium with the defocusing cubic term and fractional diffraction. This was done systematically in the numerical form, and also analytically, with the help of the TF (Thomas-Fermi) and variational approximations. The modes are characterized by the power defect ΔP and the minimum value of the field, U_{\min} . Their dependences on parameters of the system and propagation constant of the mode families, k , have been found. The computation of eigenvalues for small perturbations, as well as direct numerical simulations of the perturbed evolution, demonstrate complete stability of both the bubbles and W-shaped modes.

FUNDING

National Major Instruments and Equipment Development Project of National Natural Science Foundation of China (No. 61827815); National Natural Science Foundation of China (No. 62075138); Science and Technology Project of Shenzhen (JCYJ20190808121817100, JCYJ20190808164007485, JSGG20191231144201722); Israel Science Foundation (No. 1286/17).

CONFLICT OF INTEREST

The authors declare that they have no conflict of interest.

-
- [1] Zakharov, V.E., Manakov, S.V., Novikov, S.P., Pitaevskii, L.P.: Theory of Solitons: Inverse Scattering Transform. Nauka publishers, Moscow (1980) [English translation: Consultants Bureau, New York (1984)]
 - [2] Ablowitz, M.J., Segur, H.: Solitons and the Inverse Scattering Transform. SIAM, Philadelphia (1981)
 - [3] Dauxois, T., Peyrard, M.: Physics of Solitons. Cambridge University Press, Cambridge (2006)
 - [4] Yang, J.: Nonlinear Waves in Integrable and Nonintegrable Systems. SIAM, Philadelphia (2010)
 - [5] Kivshar, Y.S., Malomed, B.A.: Dynamics of solitons in nearly integrable systems. Rev. Mod. Phys. **61**, 763-915 (1989)
 - [6] Malomed, B.A.: Multidimensional solitons: Well-established results and novel findings. Eur. Phys. J. Spec. Top. **225**, 2507-2532 (2016)
 - [7] Kartashov, Y.V., Astrakharchik, G.E., Malomed, B.A., Torner, L.: Frontiers in multidimensional self-trapping of nonlinear fields and matter. Nat. Rev. Phys. **1**, 185-197 (2019)
 - [8] Abdullaev, F., Darmanyan, S., Khabibullaev, P.: Optical Solitons. Springer-Verlag, Berlin (1993)
 - [9] Hasegawa, A., Kodama, Y.: Solitons in Optical Communications. Clarendon Press, Oxford (1995)
 - [10] Kivshar, Y.S., Luther-Davies, B.: Dark optical solitons: physics and applications. Phys. Rep. **298**, 81-197 (1998)
 - [11] Kivshar, Y.S., Agrawal, G.P.: Optical Solitons: from Fibers to Photonic Crystals. Academic Press, San Diego (2003)
 - [12] Malomed, B.A., Mihalache, D., Wise, F., Torner, L.: Spatiotemporal optical solitons. J. Opt. B **7**, R53-R72 (2005)
 - [13] Maimistov, A.I.: Solitons in nonlinear optics. Quantum Electron. **40**, 756-781 (2010)
 - [14] Mihalache, D.: Formation and stability of light bullets: recent theoretical studies. J. Optoelect. Adv. Mat. **12**, 12-18 (2010)
 - [15] Chen, Z., Segev, M., Christodoulides, D. N.: Optical spatial solitons: historical overview and recent advances. Rep. Prog. Phys. **75**, 086401 (2012)
 - [16] Malomed, B.A., Mihalache, D.: Nonlinear waves in optical and matter-wave media: A topical survey of recent theoretical and experimental results. Rom. J. Phys. **64**, 106 (2019)
 - [17] Strecker, K.E., Partridge, G.B., Truscott, A.G., Hulet, R.G.: Bright matter wave solitons in Bose-Einstein condensates. New J. Phys. **5**, 73.1-73.8 (2003)
 - [18] Abdullaev, F.Kh., Gammal, A.G., Kamchatnov, A.M., Tomio, L.: Dynamics of bright matter wave solitons in a Bose-Einstein condensate. Int. J. Mod. Phys. B **19**, 3415-3473 (2005)
 - [19] Bagnato, V.S., Frantzeskakis, D.J., Kevrekidis, P.G., Malomed, B.A., Mihalache, D.: Bose-Einstein conden-

- sation: Twenty years after. *Rom. Rep. Phys.* **67**, 5-50 (2015)
- [20] Salasnich, L.: Bright solitons in ultracold atoms, *Opt. Quant. Electron.* **49**, 409 (2017)
- [21] Harko, T., Mak, M.K., Leung, C.S.: Vortex solutions in atomic Bose-Einstein condensates via the Adomian decomposition method. *Rom. Rep. Phys.* **72**, 116 (2020)
- [22] Passos, F.S., Dias, W.S.: From super-Bloch oscillations to sudden self-trapping in Bose-Einstein condensates with inter-atomic interactions. *Nonlinear Dyn.* **102**, 329-337 (2020)
- [23] Frantzeskakis, D.J.: Dark solitons in atomic Bose-Einstein condensates: from theory to experiments. *J. Phys. A* **43**, 213001 (2010)
- [24] Christodoulides, D.N., Carvalho, M.I.: Bright, dark, and gray spatial soliton states in photorefractive media. *J. Opt. Soc. Am. B* **12**, 1628-1633 (1995)
- [25] Kartashov, Y.V., Torner, L.: Gray spatial solitons in nonlocal nonlinear media. *Opt. Lett.* **32**, 946-948 (2007)
- [26] Chabchoub, A., Kimmoun, O., Branger, H., Kharif, C., Hoffmann, N., Onorato, M., Akhmediev, N.: Gray solitons on the surface of water. *Phys. Rev. E* **89**, 011002(R) (2014)
- [27] Gamayun, O., Bezvershenko, Yu.V., Cheianov, V.: Fate of a gray soliton in a quenched Bose-Einstein condensate. *Phys. Rev. A* **91**, 031605(R) (2015)
- [28] Efremidis, N.K., Hudock, J., Christodoulides, D.N., Fleischer, J.W., Cohen, O., Segev, M.: Two-dimensional optical lattice solitons. *Phys. Rev. Lett.* **91**, 213906 (2003)
- [29] Neshev, D., Ostrovskaya, E., Kivshar, Y., Krolikowski, W.: Spatial solitons in optically induced gratings. *Opt. Lett.* **28**, 710-712 (2003)
- [30] Fleischer, J.W., Segev, M., Efremidis, N.K., Christodoulides, D. N.: Observation of two-dimensional discrete solitons in optically induced nonlinear photonic lattices. *Nature* **422**, 147-150 (2003)
- [31] Kartashov, Y.V., Egorov, A.A., Torner, L., Christodoulides, D.N.: Stable soliton complexes in two-dimensional photonic lattices. *Opt. Lett.* **29**, 1918-1920 (2004)
- [32] Mihalache, D., Mazilu, D., Lederer, F., Kivshar, Y.S.: Collisions between discrete surface spatiotemporal solitons in nonlinear waveguide arrays. *Phys. Rev. A* **79**, 013811 (2009)
- [33] Brazhnyi, V.A., Konotop, V.V.: Theory of nonlinear matter waves in optical lattices. *Mod. Phys. Lett. B* **18**, 627-651 (2004)
- [34] Mihalache, D., Mazilu, D., Lederer, F., Kartashov, Y.V., Crasovan, L.C., Torner, L.: Stable three-dimensional spatiotemporal solitons in a two-dimensional photonic lattice. *Phys. Rev. E* **70**, 055603 (2004)
- [35] Morsch, O., Oberthaler, M.: Dynamics of Bose-Einstein condensates in optical lattices. *Rev. Mod. Phys.* **78**, 179-215 (2006)
- [36] Kartashov, Y.V., Vysloukh, V.A., Torner, L.: Soliton shape and mobility control in optical lattices. *Prog. Opt.* **52**, 63-148 (2009)
- [37] Kartashov, Y.V., Vysloukh, V.A., Torner, L.: Solitons in complex optical lattices. *Eur. Phys. J. Spec. Top.* **173**, 87-105 (2009)
- [38] Zeng, L., Zeng, J.: Gap-type dark localized modes in a Bose-Einstein condensate with optical lattices. *Adv. Photon.* **1**, 046004 (2019)
- [39] Zhang, Y., Wu, B.: Composition Relation between Gap Solitons and Bloch Waves in Nonlinear Periodic Systems. *Phys. Rev. Lett.* **102**, 093905 (2009)
- [40] Rose, P., Richter, T., Terhalle, B., Imbrock, J., Kaiser, F., Denz, C.: Discrete and dipole-mode gap solitons in higher-order nonlinear photonic lattices. *Appl. Phys. B* **89**, 521-526 (2007)
- [41] Malomed, B.A., Kevrekidis, P.G.: Discrete vortex solitons. *Phys. Rev. E* **64**, 026601 (2001)
- [42] Baizakov, B.B., Malomed, B.A., Salerno, M.: Multi-dimensional solitons in periodic potentials. *Europhys. Lett.* **63**, 642-648 (2003)
- [43] Yang, J., Musslimani, Z.H.: Fundamental and vortex solitons in a two-dimensional optical lattice. *Opt. Lett.* **28**, 2094-2096 (2003)
- [44] Baizakov, B.B., Malomed, B.A., Salerno, M.: Multidimensional solitons in a low-dimensional periodic potential. *Phys. Rev. A* **70**, 053613 (2004)
- [45] Yang, J.: Stability of vortex solitons in a photorefractive optical lattice. *New J. Phys.* **6**, 47 (2004)
- [46] Kartashov, Y.V., Malomed, B.A., Torner, L.: Solitons in nonlinear lattices. *Rev. Mod. Phys.* **83**, 247-306 (2011)
- [47] Kartashov, Y.V., Vysloukh, V.A., Torner, L.: Propagation of solitons in thermal media with periodic nonlinearity. *Opt. Lett.* **33**, 1774-1776 (2008)
- [48] Kartashov, Y.V., Malomed, B.A., Vysloukh, V.A., Torner, L.: Two-dimensional solitons in nonlinear lattices. *Opt. Lett.* **34**, 770-772 (2009)
- [49] Abdullaev, F.Kh., Kartashov, Y.V., Konotop, V.V., Zezyulin, D.A.: Solitons in \mathcal{PT} -symmetric nonlinear lattices. *Phys. Rev. A* **83**, 041805(R) (2011)
- [50] Borovkova, O.V., Kartashov, Y.V., Torner, L., Malomed, B.A.: Bright solitons from defocusing nonlinearities. *Phys. Rev. E* **84**, 035602(R) (2011)
- [51] Borovkova, O.V., Kartashov, Y.V., Malomed, B.A., Torner, L.: Algebraic bright and vortex solitons in defocusing media. *Opt. Lett.* **36**, 3088-3090 (2011)
- [52] Dror, N., Malomed, B.A.: Solitons and vortices in nonlinear potential wells. *J. Opt.* **16**, 014003 (2016)
- [53] Lobanov, V.E., Borovkova, O.V., Kartashov, Y.V., Malomed, B.A., Torner, L.: Stable bright and vortex solitons in photonic crystal fibers with inhomogeneous defocusing nonlinearity. *Opt. Lett.* **37**, 1799-1801 (2012)
- [54] Tian, Q., Wu, L., Zhang, Y., Zhang, J.-F.: Vortex solitons in defocusing media with spatially inhomogeneous nonlinearity. *Phys. Rev. E* **85**, 056603 (2012)
- [55] Wu, Y., Xie, Q., Zhong, H., Wen, L., Hai, W.: Algebraic bright and vortex solitons in self-defocusing media with spatially inhomogeneous nonlinearity. *Phys. Rev. A* **87**, 055801 (2013)
- [56] Driben, R., Kartashov, Y.V., Malomed, B.A., Meier, T., Torner, L.: Three-dimensional hybrid vortex solitons. *New J. Phys.* **16**, 063035 (2014)
- [57] Driben, R., Kartashov, Y.V., Malomed, B.A., Meier, T., Torner, L.: Soliton gyroscopes in media with spatially growing repulsive nonlinearity. *Phys. Rev. Lett.* **112**, 020404 (2014)
- [58] Kartashov, Y.V., Malomed, B.A., Shnir, Y., Torner, L.: Twisted toroidal vortex solitons in inhomogeneous media with repulsive nonlinearity. *Phys. Rev. Lett.* **113**, 264101 (2014)

- [59] Kartashov, Y.V., Malomed, B.A., Vysloukh, V.A., Belić, M.R., Torner, L.: Rotating vortex clusters in media with inhomogeneous defocusing nonlinearity. *Opt. Lett.* **42**, 446-449 (2017)
- [60] Zeng, L., Zeng, J.: Modulated solitons, soliton and vortex clusters in purely nonlinear defocusing media. *Ann. Phys.* **421**, 168284 (2020)
- [61] Zeng, L., Zeng, J., Kartashov, Y.V., Malomed, B.A.: Purely Kerr nonlinear model admitting flat-top solitons. *Opt. Lett.* **44**, 1206-1209 (2019)
- [62] Zeng, L., Zeng, J.: Gaussian-like and flat-top solitons of atoms with spatially modulated repulsive interactions. *J. Opt. Soc. Am. B* **36**, 2278-2284 (2019)
- [63] Barashenkov, I.V., Panova, E.Y.: Stability and evolution of the quiescent and traveling solitonic bubbles. *Physica D* **69**, 114-134 (1993)
- [64] Becker, C., Sengstock, K., Schmelcher, P., Kevrekidis, P.G., Carretero-González, R.: Inelastic collisions of solitary waves in anisotropic Bose-Einstein condensates: sling-shot events and expanding collision bubbles. *New J. Phys.* **15**, 113028 (2013)
- [65] Varga, R., Paal, G.: Numerical investigation of the strength of collapse of a harmonically excited bubble. *Chaos Solitons Fract.* **76**, 56-71 (2015)
- [66] Zhao, L.-C., Li, S.-C., Ling, L.: Rational W-shaped solitons on a continuous-wave background in the Sasa-Satsuma equation. *Phys. Rev. E* **89**, 023210 (2014)
- [67] Zhao, L.-C., Li, S.-C., Ling, L.: W-shaped solitons generated from a weak modulation in the Sasa-Satsuma equation. *Phys. Rev. E* **93**(3), 032215 (2016)
- [68] Wang, X., Liu, C., Wang, L.: Rogue waves and W-shaped solitons in the multiple self-induced transparency system. *Chaos* **27**, 093106 (2017)
- [69] Triki, H., Porsezian, K., Choudhuri, A., Dinda, P.T.: W-shaped, bright and kink solitons in the quadratic-cubic nonlinear Schrödinger equation with time and space modulated nonlinearities and potentials. *J. Mod. Opt.* **63**, 1368-1376 (2017)
- [70] Bendahmane, I., Triki, H., Biswas, A., Alshomrani, A.S., Zhou, Q., Moshokoa, S.P., Belić, M.: Bright, dark and W-shaped solitons with extended nonlinear Schrödinger equation for odd and even higher-order terms. *Superlattice Microst.* **114**, 53-61 (2018)
- [71] Triki, H., Bensalem, C., Biswas, A., Zhou, Q., Ekici, M., Moshokoa, S.P., Belić, M.: W-shaped and bright optical solitons in negative indexed materials. *Chaos Solitons Fract.* **123**, 101-107 (2019)
- [72] Triki, H., Zhou, Q., Liu, W.: W-shaped solitons in inhomogeneous cigar-shaped Bose-Einstein condensates with repulsive interatomic interactions. *Laser Phys.* **29**, 055401 (2019)
- [73] Laskin, N.: Fractional quantum mechanics and Lévy path integrals. *Phys. Lett. A* **268**, 298-305 (2000)
- [74] Laskin, N.: Fractional quantum mechanics. *Phys. Rev. E* **62**, 3135-3145 (2000)
- [75] Laskin, N.: Fractional Schrödinger equation. *Phys. Rev. E* **66**, 056108 (2002)
- [76] Laskin, N.: Fractional quantum mechanics. World Scientific, Singapore (2018)
- [77] Zhang, Y.Q., Liu, X., Belić, M.R., Zhong, W.P., Zhang, Y.P., Xiao, M.: Propagation dynamics of a light beam in a fractional Schrödinger equation. *Phys. Rev. Lett.* **115**, 180403 (2015)
- [78] Guo, B., Li, Q.: Existence of the global smooth solution to a fractional nonlinear Schrödinger system in atomic Bose-Einstein condensates. *J. Appl. Anal. Comp.* **5**, 793-808 (2015)
- [79] Stickler, B.A.: Potential condensed-matter realization of space-fractional quantum mechanics: The one-dimensional Lévy crystal. *Phys. Rev. E* **88**, 012120 (2013)
- [80] Pinsker, F., Bao, W., Zhang, Y., Ohadi, H., Dreismann, A., Baumberg, J.J.: Fractional quantum mechanics in polariton condensates with velocity-dependent mass. *Phys. Rev. B* **92**, 195310 (2015)
- [81] Longhi, S.: Fractional Schrödinger equation in optics. *Opt. Lett.* **40**, 1117-1120 (2015)
- [82] Zhong, W.P., Belić, M.R., Malomed, B.A., Zhang, Y., Huang, T.: Spatiotemporal accessible solitons in fractional dimensions. *Phys. Rev. E* **94**, 012216 (2016)
- [83] Zhong, W.P., Belić, M.R., Zhang, Y.: Accessible solitons of fractional dimension. *Ann. Phys.* **368**, 110-116 (2016)
- [84] Zeng, L., Zeng, J.: One-dimensional solitons in fractional Schrödinger equation with a spatially periodical modulated nonlinearity: nonlinear lattice. *Opt. Lett.* **44**, 2661-2664 (2019)
- [85] Wang, Q., Deng, Z.Z.: Elliptic Solitons in (1+2)-Dimensional Anisotropic Nonlocal Nonlinear Fractional Schrödinger Equation. *IEEE Photonics J.* **11**, 1-8 (2019)
- [86] Li, P., Li, J., Han, B., Ma, H., Mihalache, D.: \mathcal{PT} -symmetric optical modes and spontaneous symmetry breaking in the space-fractional Schrödinger equation. *Rom. Rep. Phys.* **71**, 106 (2019)
- [87] Li, P., Dai C.: Double Loops and Pitchfork Symmetry Breaking Bifurcations of Optical Solitons in Nonlinear Fractional Schrödinger Equation with Competing Cubic-Quintic Nonlinearities, *Ann. Phys. (Berlin)* **532**, 2000048 (2020)
- [88] Li, P., Malomed, B.A., Mihalache, D.: Symmetry breaking of spatial Kerr solitons in fractional dimension. *Chaos Solitons Fract.* **132**, 109602 (2020)
- [89] Chen, J., Zeng, J.: Spontaneous symmetry breaking in purely nonlinear fractional systems. *Chaos* **30**, 063131 (2020)
- [90] Zeng, L., Zeng, J.: One-dimensional gap solitons in quintic and cubic-quintic fractional nonlinear Schrödinger equations with a periodically modulated linear potential. *Nonlinear Dyn.* **98**, 985-995 (2019)
- [91] Li, P., Malomed, B.A., Mihalache, D.: Vortex solitons in fractional nonlinear Schrödinger equation with the cubic-quintic nonlinearity. *Chaos Solitons Fract.* **137**, 109783 (2020)
- [92] Wang, Q., Liang, G.: Vortex and cluster solitons in nonlocal nonlinear fractional Schrödinger equation. *J. Opt.* **22**, 055501 (2020)
- [93] Qiu, Y., Malomed, B.A., Mihalache, D., Zhu, X., Peng, X., He, Y.: Stabilization of single- and multi-peak solitons in the fractional nonlinear Schrödinger equation with a trapping potential. *Chaos Solitons Fract.* **140**, 110222 (2020)
- [94] Zeng, L., Zeng, J.: Preventing critical collapse of higher-order solitons by tailoring unconventional optical diffraction and nonlinearities. *Commun. Phys.* **3**, 26 (2020)
- [95] Li, P., Malomed, B.A., Mihalache, D.: Metastable soliton necklaces supported by fractional diffraction and

- competing nonlinearities. *Opt. Express* **28**, 34472-33488 (2020)
- [96] Zeng, L., Zeng, J.: Fractional quantum couplers. *Chaos Solitons Fract.* **140**, 110271 (2020)
- [97] Zeng, L., Shi, J., Lu, X., Cai, Y., Zhu, Q., Chen, H., Long, H., Li, J.: Stable and oscillating solitons of \mathcal{PT} -symmetric couplers with gain and loss in fractional dimension. *Nonlinear Dyn.* **103**, 1831-1840 (2021)
- [98] Molina, M.I.: The fractional discrete nonlinear Schrödinger equation. *Phys. Lett. A* **384**, 126180 (2020)
- [99] Zeng, L., Mihalache, D., Malomed, B.A., Lu, X., Cai, Y., Zhu, Q., and Li, J.: Families of fundamental and multipole solitons in a cubic-quintic nonlinear lattice in fractional dimension. *Chaos Solitons Fract.* **144**, 110589 (2021)
- [100] Qiu, Y., Malomed, B.A., Mihalache, D., Zhu, X., Zhang, L., He, Y.: Soliton dynamics in a fractional complex Ginzburg-Landau model. *Chaos Solitons Fract.* **131**, 109471 (2020)
- [101] Kasprzak, H.: Differentiation of a noninteger order and its optical implementation. *Appl. Opt.* **21**, 3287-3291 (1982)
- [102] Davis, J.A., Smith, D.A., McNamara, D.E., Cottrell, D.M., Campos, J.: Fractional derivatives—analysis and experimental implementation. *Appl. Opt.* **40**, 5943-5948 (2020)
- [103] Pitaevskii, L.P., Stringari, S.: *Bose-Einstein Condensation*. Oxford University Press, Oxford (2003)